Review

Recent Developments in Synthesis and Photocatalytic Applications of Carbon Dots

Chularat Sakdaronnarong [1], **Amornrat Sangjan** [1], **Suthida Boonsith** [1], **Dong Chung Kim** [2,*] **and Hyeon Suk Shin** [3,4,5,*]

1 Department of Chemical Engineering, Faculty of Engineering, Mahidol University, Nakhon Pathom 73170, Thailand; chularat.sak@mahidol.ac.th (C.S.); amornrat.sag@student.mahidol.ac.th (A.S.); suthida.bos@mahidol.ac.th (S.B.)
2 Department of Chemical Engineering, Chungwoon University, Incheon 22100, Korea
3 Department of Energy Engineering, Ulsan National Institute of Science & Technology (UNIST), Ulsan 44919, Korea
4 Department of Chemistry, UNIST, Ulsan 44919, Korea
5 Low Dimensional Carbon Material Center, UNIST, Ulsan 44919, Korea
* Correspondence: kimdc@chungwoon.ac.kr (D.C.K.); shin@unist.ac.kr (H.S.S.)

check for updates

Abstract: The tunable photoluminescent and photocatalytic properties of carbon dots (CDs) via chemical surface modification have drawn increased attention to this emerging class of carbon nanomaterials. Herein, we summarize the advances in CD synthesis and modification, with a focus on surface functionalization, element doping, passivation, and nanocomposite formation with metal oxides, transition metal chalcogenides, or graphitic carbon nitrides. The effects of CD size and functionalization on photocatalytic properties are discussed, along with the photocatalytic applications of CDs in energy conversion, water splitting, hydrogen evolution, water treatment, and chemical degradation. In particular, the enzyme-mimetic and photodynamic applications of CDs for bio-related uses are thoroughly reviewed.

Keywords: carbon dots; functionalization; nanocomposites; photocatalysis; photoluminescence; enzyme

---

1. Introduction to Carbon Dots (CDs)

Carbon dots (CDs) are discrete quasi-spherical carbon particles with sizes of <10 nm, normally having an sp^2-conjugated carbon core with oxygenated functional groups, such as –OH, –COOH, and –CHO. The salient feature of CDs is their photoluminescence (PL), specifically, their excitation wavelength-(in)dependent emission [1]. Since 2006, CDs have been extensively researched due to their simple synthesis, low cost, abundance, excellent biocompatibility, and other advantages, and they have found diverse applications in the fields of (photo) catalysis, optoelectronics, energy storage/conversion, nanomedicine, sensing, and bioimaging [2]. More than half of these applications make use of the photoresponsive ability of CDs in a wide wavelength (ultraviolet to infrared) range and their outstanding electron transfer performance. The low toxicity and biocompatibility of CDs make them viable alternatives to heavy metal-based semiconducting quantum dots (QDs). Although the wide application scope of CDs necessitates the development of suitable large-scale synthesis methods, only few works have dealt with the mass production of CDs, as the ease of large-scale synthesis depends strongly on the intrinsic nature of raw materials [3].

2. Synthesis of CDs

CDs, which were first discovered in 2004 during carbon nanotube purification [4], exhibit well-pronounced and tunable fluorescent properties, additionally featuring the benefits of small size, biocompatibility, high photostability, electro-chemiluminescence, tunable photoluminescence, and excellent multi-photon excitation. It was found that carbon dots are also able to absorb multiple photons and they emit similar emission wavelength. This characteristic facilitates the bio-application of CDs for in vivo bio-imaging in viable cells containing various cellular organs while using infrared spectra. Consequently, CDs have low toxicity, are chemically inert, and can be surface-functionalized with biomolecules to allow for biological imaging and drug delivery applications [5,6].

CD syntheses can be classified into those that are based on top-down and bottom-up techniques. In the former case, bulk carbon precursors, such as graphite rods, candle soot, and fullerenes, are broken down into smaller particles (<10 nm) by harsh methods, such as chemical/laser ablation, electrochemical carbonization, and microwave exfoliation [7]. Conversely, the latter techniques rely on the carbonization, condensation, and polymerization of the basic building blocks of carbon precursors (e.g., corncob [8], β-cyclodextrin [9], cellulose [10,11], milk [12], citric acid [13], and algae [14]) that are induced by microwave irradiation and hydro-/solvothermal treatment to afford fluorescent CDs [15]. Specifically, the hydro-/solvothermal methods of CD synthesis are fast, easily scalable, cost-effective, environmentally friendly, and provide high quantum yields (QYs), therefore enjoying popularity [16]. Figure 1 illustrates the abovementioned CD synthesis techniques.
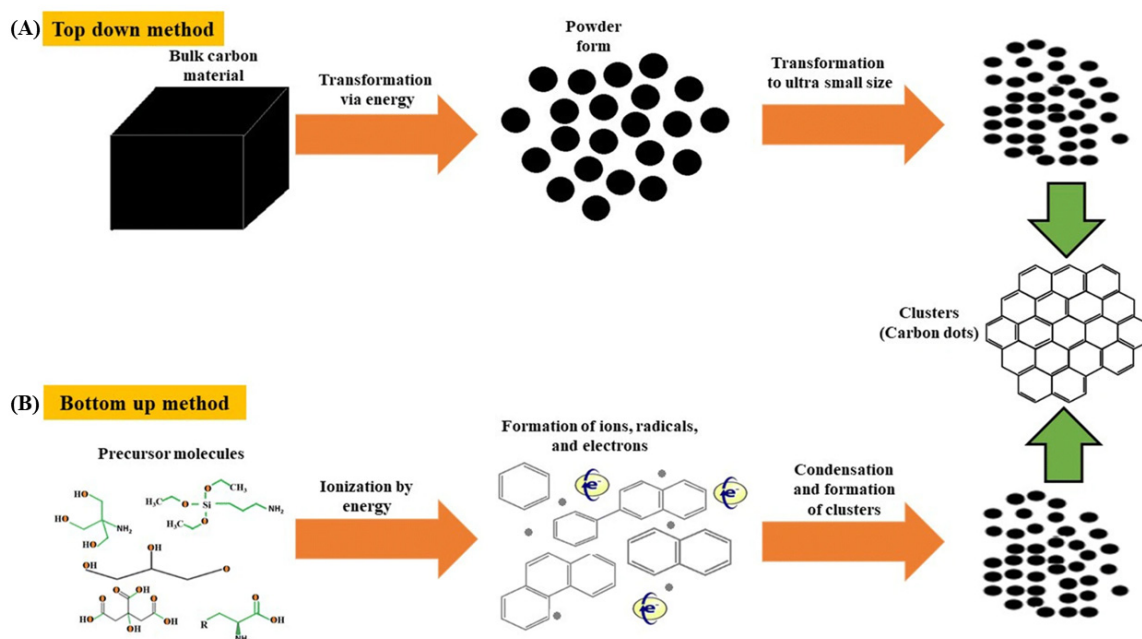

Figure 1. Synthesis of carbon dots by (**A**) top-down and (**B**) bottom-up methods; Reproduced with permission from [15] published by Springer Nature, 2019.

This review focuses on scalable bottom-up CD syntheses offering the benefits of precisely controllable morphology and size distribution, as well as convenient surface passivation. The widespread hydrothermal CD synthesis techniques employ various organic molecules as precursors. Ana and Camacho [10] used two different cellulose-based materials, raw cellulose (RC) and nanocrystalline cellulose (NC), which were extracted from the green algae (*Cladophora rupestris*) as carbon sources to probe the effect of precursor size on the properties of CDs that were intended for application in solar cells. RC comprises compact amorphous fibers with a diameter of 0.53 ± 0.09 μm, while NC has a loose crystalline structure, containing particles with a diameter of 20.0 ± 4.4 nm. Notably, RC afforded smaller CDs (10.0 ± 3.74 nm) than NC (76.9 ± 73.1 nm), even though the former

precursor had a larger particle size than the latter. This finding was mainly ascribed to the fact that the synthesis of CDs from NC was performed at a higher concentration, which favored the aggregation or clustering of the hydrophilic-surface CDs. RC- and NC-derived CDs both exhibited strong green luminescence at ~540 nm upon excitation at 365 nm. In another work, smaller CDs with an average diameter of 6 nm were hydrothermally prepared from red lentils [17] and they were shown to exhibit an amorphous graphitic structure, as follows from the X-ray diffraction peak at $2\theta = 22°$. The strong blue (448 nm, excitation at 360 nm) fluorescence of these CDs was quenched by Fe^{3+}, which allowed them to be used as a sensor for this ion.

CDs can also be prepared by various methods, such as microwave-assisted, reflux, rapid heating, and electrochemical processes. Rai et al. [18] studied the effect of lignosulfonate lignin concentration on the properties of CDs that were synthesized from the above substrate by a microwave-assisted technique. CDs that were obtained after dialysis had an average diameter of 4.6 nm, and their mass yields and fluorescence emission wavelengths were affected by the lignin precursor concentration. The color of photoluminescence under both short-wavelength (254 nm) and long-wavelength (365 nm) UV irradiation changed after reduction with $NaBH_4$ to more intense light green and more contrast green luminescence, respectively. After microwave treatment, the aromatization and creation of aromatic clumps of lignin fragments take place via various reactions (aldol condensation and cyclo addition), and CDs are formed when it reaches a critical saturation position. Acid oxidation yielded CDs with various oxidized functional groups (OH, COOH, SO_3, C = O) on surface and further $NaBH_4$ reduction enhances CDs contrast and intense green luminescence attributed to modulation or reducing the functional groups of the surface residues. Yang et al. [19] used microwave treatment to synthesize water-soluble CDs with an average size of ~4 nm and high biocompatibility, achieving a high QY of ~25%. In addition, reflux methods are widely used for CD production. Wang et al. [20] synthesized multicolor CDs by a one-step reaction of L-cysteine and D-galactose upon reflux, showing that multicolor properties could be controlled by varying the concentration of NaOH. Yellow (10.4 ± 1.2 nm), green (6.1 ± 0.6 nm), and blue (3.3 ± 0.5 nm) CDs were produced in the presence of 0.1, 0.2, and 0.4 M NaOH, respectively, i.e., CD size decreased with increasing NaOH concentration, which was ascribed to the concomitant slowdown of isotropic growth. In another work, CDs were prepared from bleached eucalyptus kraft pulp by simple reflux in concentrated H_2SO_4, followed by oxidation with HNO_3 [21]. These quasi-spherical CDs had diameters of 1–3 nm and featured abundant oxygenated functional groups (e.g., –COOH, –OH, –C = O, –NO_2) on their surface. Surface passivation with thionyl chloride followed by polyethylene glycol (PEG) treatment increased QY from 1.2 to 3.2%, with maximum photoluminescence intensity being achieved at 450 nm (blue/green luminescence) under excitation at 340 nm. CDs with multicolor fluorescence were prepared from mango peel by numerous methods, e.g., hydrothermal treatment, pyrolysis, and direct oxidation in concentrated H_2SO_4 [22]. CDs that were synthesized by pyrolysis had the highest QY (4.1%), while those prepared by hydrothermal and direct oxidation methods had QYs of 0.6 and 0.2%, respectively. However, the combination of pyrolysis and direct oxidation provided CDs with an even higher QY of 8.5%. The synthesized CDs were nearly spherical and had sizes of 2–6 nm, additionally containing abundant surface hydrophilic groups (e.g., hydroxyl, carbonyl, carboxyl, and amino ones) accounting for compatibility with aqueous solutions.

A recent study employed a bottom-up electrochemical process to precisely manipulate CD morphology and size [23]. CDs with an average size of 3.02 ± 0.12 nm were produced from an ionic liquid methylimidazolium hexafluorophosphate ($BMIMPF_6$)/acetonitrile mixture by an electrochemical method (Figure 2A,B), and an extremely high QY of 11.6% was achieved at an applied potential of 15 V. The above CDs featured an absorption peak at 278 nm, which was attributed to the π-π* transition of aromatic sp^2 carbons (Figure 2C), and exhibited blue luminescence (excitation at 365 nm). Regarding photoluminescence, the maximum emission at 422 nm (blue/green luminescence) was obtained for excitation at 355 nm. Transmission electron microscopic (TEM), high resolution transmission electron

microscope (HR-TEM), and atomic force microscopic (AFM) images of CDs that were synthesized from BMIMPF$_6$/acetonitrile at ratio of 1: 500 are illustrated in Figure 2D–F, respectively.
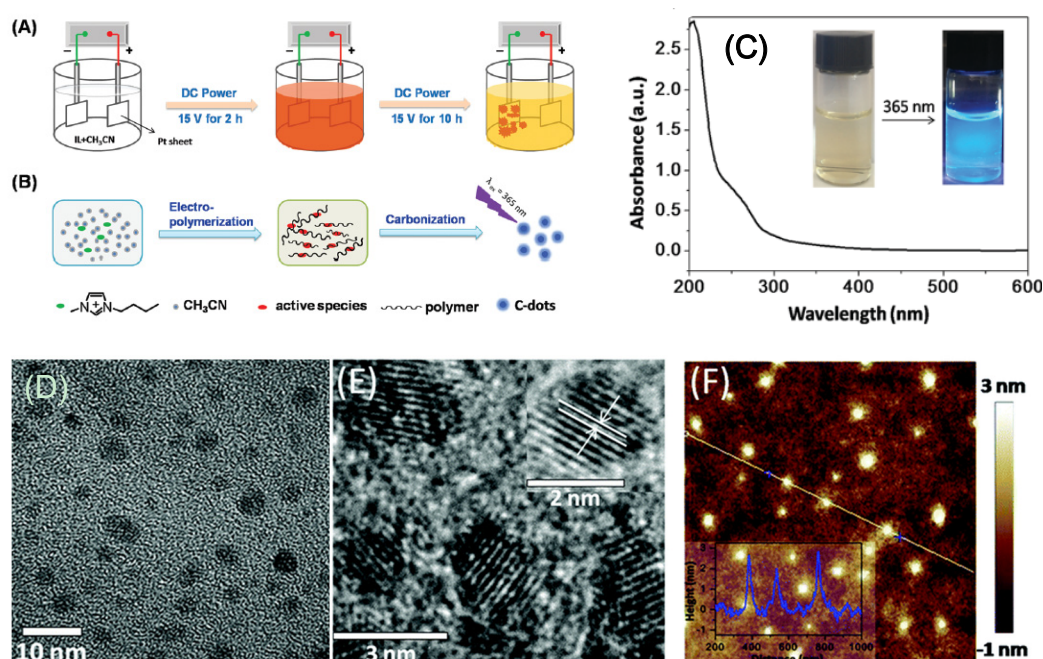

Figure 2. (**A**) Schematic illustration for carbon dot (CD) synthesis via the electrochemical strategy. (**B**) Mechanism of CD synthesis. (**C**) UV-VIS absorption spectrum of CD. In the inset, left and right photographs were for as-synthesized CDs under visible and UV (excited at 365 nm) light, respectively. (**D**) Transmission electron microscopic (TEM), (**E**) high resolution transmission electron microscope (HR-TEM), and (**F**) atomic force microscopic (AFM) topography images of CDs synthesized from BMIMPF$_6$/acetonitrile at ratio of 1:500 on a silicon substrate with a height profile (inset)—Reproduced with permission from [23] published by The Royal Society of Chemistry, 2016.

A simple and rapid heating method was used to obtain CDs with QYs of up to 30% [9] from oligoethylenimine and β-cyclodextrin by incubation in a phosphoric acid/water mixture at 90 °C for only 2 h. CDs that were obtained after dialysis had a uniform spherical shape with diameters of 2–4 nm and they exhibited outstanding green fluorescence at 510 nm (excitation at 390 nm) with a QY of 30%. Table 1 summarizes methods of CD synthesis from different precursors as well as CD optical/physical properties and applications.

Table 1. Summary of precursors, synthesis methods, particle size, and optical properties, as well as applications of synthesized carbon dots.

Precursor	Synthesis method	Conditions	Quantum yield (QY)	Fluorescence color	Particle size	Application	Ref
Cellulose from *Cladophora rupestris*	Hydrothermal	220 °C, 6 h	-	Green (~540 nm)	5.79 ± 1.60 nm	solar cell sensitization	[10]
Lignin	Microwave irradiation	600 W, 10 min	-	Blue (475 nm)	4.6 nm	Bioimaging	[18]
L-cysteine and D-(+)-galactose	One-step refluxing	80 °C, 24 h	-	Yellow (550 nm), green (495 nm) and blue (400 nm)	3.3–10.4 nm	Detection of caffeine, melamine, and fenitrothion	[20]
Oligoethylenimine (OEI), β-cyclodextrin and phosphoric acid	Simple fast heating	90 °C, 2 h	30%	Green (510 nm)	2–4 nm	Bioimaging and theranostic carrier	[9]
Red lentils	Hydrothermal reaction	200 °C, 5 h	13.2%	Blue (448 nm)	6 nm	Detection of Fe^{3+}	[17]
Acetonitrile and ionic liquid	Electrochemical	Potential: 5–20 V, Ionic liquid/Acetronitrile ratio: 1:10–1:1000	Max 13.3%	Blue (422 nm)	3.02 ± 0.12 nm (15 V potential and 1:500 Ionic liquid:acetronitrile)	ferric ion detection and cell imaging	[23]
Cellulose, Urea, and NaOH	Hydrothermal reaction	Vary temp: 140–300 °C, Vary time: 1–24 h	Max 10.9% (300 °C)	-	3.8 nm	Detection of Fe^{3+}	[11]
Milk	Hydrothermal reaction	180 °C, 2 h	-	Blue (444 nm)	10 nm	Drug delivery	[12]
Corncob	Hydrothermal reaction	180 °C, 5 h	-	-	9.31 nm	Detection of metal ion	[8]
Folic acid and urea	Microwave irradiation	500 W, 8 min	-	Blue (460 nm)	1–7 nm	Cancer cell detection	[19]
Cellulose, sulfuric acid, and nitric acid	Reflux	12 h	3.2%	Blue (450 nm)	2 nm	-	[21]

Patents involving CDs synthesis and applications are few, as most related research deals with the synthesis and applications of metal-containing QDs. The first CD-related patent (filed in 2010) describes a method of producing water-soluble fluorescent carbon dots from carbon soot [24]. CDs with sizes of 2–7 nm were oxidatively treated to introduce hydrophilic surface carboxyl groups in amounts that are sufficient for fluorescence [24]. Another patent disclosed a single-step hydrothermal method of preparing water-soluble biomass-derived fluorescent CDs from cellulose and urea [25]. The prepared CDs were subjected to centrifugation, dialysis, and lyophilization to obtain solid-state CDs, which showed promising water solubility, low toxicity, good biocompatibility, and could be potentially used for cell imaging [25]. The recently described production of nitrogen-doped fluorescent CDs from milk at a moderate temperature (100–120 °C) within a short time (20–40 min.) [26] paves the way to the low-cost large-scale production of fluorescent CDs with a size distribution of 2–10 nm. In 2017, two patents describing the preparation of biomass-derived CDs were filed [27,28]. One of these patents describes a method comprising the consecutive steps of biomass impregnation and hydrothermal carbonization for 1–5 h at 150–350 °C in the presence of one or more activators, such as KOH, NaOH, K_2CO_3, $KHCO_3$, Na_2CO_3, and $NaHCO_3$ [27], which affords CDs with a uniform size distribution and an average size of 5 nm. Another patent describes the synthesis of biomass tar–derived CDs via a catalytic reaction of a molecular sieve/tar mixture at 300–800 °C, followed by sonication [28], which provides well-dispersed CDs with a high QY. The categories of patents that are related to CDs are illustrated by the overall patent analysis and international patent classification (IPC) groups presented in Figure 3A. The top groups of filed patents and the numbers of filed patents, as demonstrated in Figure 3B, involve chemistry/metallurgy containing carbon, modified nanoparticles utilizing carbon source, co-doped carbon, biomass hydrothermal, and microwave synthesis for sun-light excitable carbon dots, as well as the application of CDs exhibiting luminescence, e.g., electroluminescence, chemiluminescence, photonics, and sensors, as well as CDs that are suitable for bio-related applications, such as imaging, dressing, and photothermal treatment.

In summary, the control of CD size, precursor dimensions, and additional chemicals, as well as their concentration to slow down the isotropic growth of particles, play crucial roles apart from synthesis conditions (e.g., temperature and time). CD photoluminescent properties can be effectively enhanced by reduction/oxidation with proper agents (e.g., $NaBH_4$, nitric acid, and phosphoric acid). The size and reduction degree of CDs influence the blue shift of their fluorescence peaks, owing to the effects of surface plasmon resonance and quantum confinement. However, post-treatment and purification are required to obtain CDs with high stability, excellent QY, a narrow size distribution, and, hence, superior photoluminescent, optoelectronic, and photocatalytic properties.
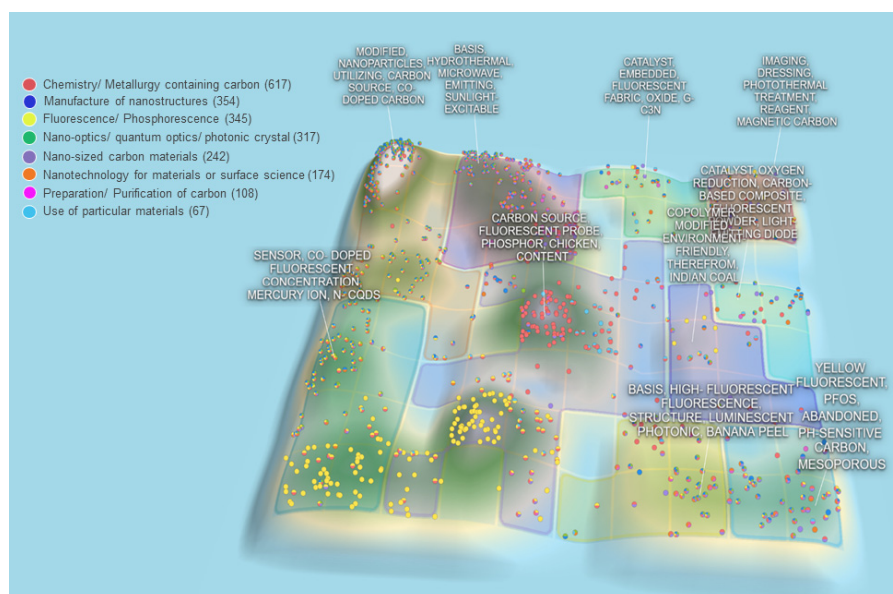
(A)
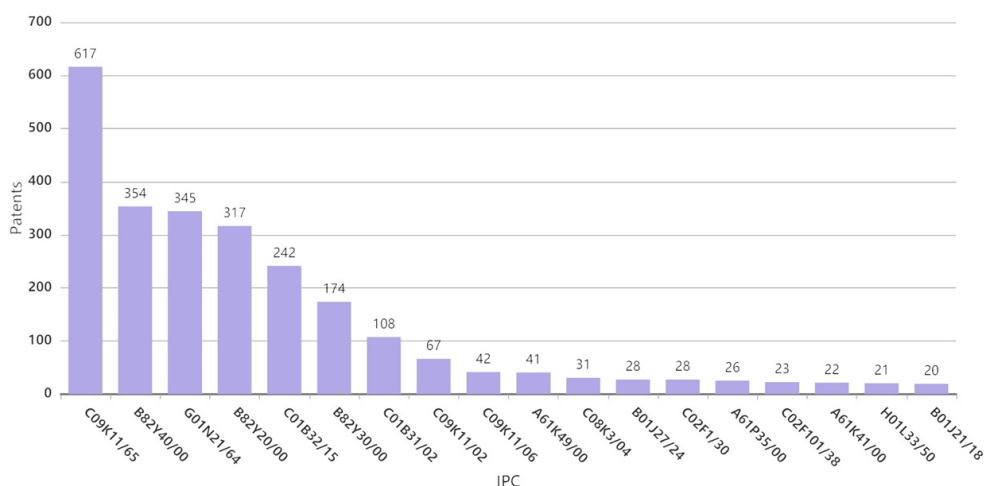
(B)

Figure 3. (**A**) Patent landscape on CDs and (**B**) the numbers of patent and patent applications according to the top international patent classification (IPC) groups analyzed by PatSnap in February 2020.

3. Modification and Photocatalytic Applications of CDs

The need for green, sustainable, and circular syntheses of chemicals and fuels has drawn much attention to photocatalytic processes, in which solar energy drives redox reactions. The band-gap structure and charge transfer ability of the corresponding photocatalyst is a vital factor influencing the efficiency of a given reaction. Thus, the diversity and controllability of CD properties have inspired numerous works on the photocatalytic applications of CDs.

Photocatalytic processes comprise the stages of (i) light absorption and electron-hole pair generation, (ii) charge migration and transfer toward the photocatalyst surface, and (iii) incident reduction and oxidation at the photocatalyst surface due to the carried charges [29]. The spontaneous redox reactions occur at the photocatalyst surface. The rapid recombination of electrons and holes takes place, unless either oxygen or other electron acceptors scavenge the electrons to generate superoxide ($O_2^{\bullet-}$) and perhydroxyl ($HOO^{\bullet}$) radicals and, subsequently, H_2O_2 [30].

Band gap energy is of utmost importance in the design of high-performance photocatalysts, as this parameter needs to be equal to or lower than photon energy for the photocatalyst to be effective. As TiO$_2$ is a photocatalyst with wide band gap, it can only be excited by short-wavelength UV radiation. One should design photocatalysts absorbing light in a broad range of wavelengths, especially at visible-light or longer ones, to enhance the efficiency of solar light utilization. Visible light corresponds to photons with energies of 2.43–3.2 eV and, thus, the bandgap of visible-light-excitable photocatalysts should be less than the aforementioned photon energy [29]. Moreover, the photocatalyst valence band energy should be more positive than the oxidation potential, while the conduction band energy should be more negative than the reduction potential. The inherent electron-hole pair generation and migration toward the photocatalyst surface, as well as the photocatalyst surface states that facilitate charge trapping and transport, can substantially enhance photocatalytic performance. Consequently, the surface passivation and functionalization of photocatalysts are essential not only for increasing their efficiency, but also for enhancing their resistance to corrosion and dissociation that are caused by photogenerated intermediates [31].

3.1. Modification of CDs for Photocatalysis

The photocatalytic properties of CDs were first discovered in 2010 [32]: CDs that were synthesized by an alkali-assisted electrochemical method and featuring diameters of 1.2–3.8 nm showed outstanding size-dependent photoluminescent properties [32]. However, CD surface modification, the grafting of CDs onto other semiconductor photocatalysts, and/or composite formation are required to make CDs suitable for use as photocatalysts or photosensitizers.

Based on literature studies, the methods of modifying CDs for photocatalytic applications can be categorized into surface functionalization, passivation, element doping, and composite synthesis. Figure 4 illustrates the difference between CD surface functionalization and passivation. The surface functionalization of photocatalysts or photosensitizers can facilitate the separation of electrons and holes, prevent their recombination, and promote charge migration by trapping the photogenerated electrons at a variety of surface sites, which allows for one to control the kinetics of redox reactions. Various methods have been introduced to manipulate the surface functionalization of CDs, as exemplified by coordination/complexation techniques [33], sol-gel techniques [34], covalent bonding strategies, such as amide coupling [35], and π-π interactions [36]. Among the functionalization techniques, acyl chloride ligand exchange replaces carboxyl groups on the CD surface with amine groups. Typically, carboxyl-capped CDs that were hydrothermally synthesized from organic acids [37,38] are reacted with thionyl chloride under reflux to selectively convert surface carboxyl groups into acyl chloride groups and, thus, make CDs soluble in polar organic solvents, such as acetone, tetrahydrofuran, and acetonitrile. Thus, this functionalization facilitates the simple purification of CDs by solvent extraction [39], and the highly reactive acyl chloride groups can be additionally replaced with amine groups. In turn, the amino groups can be reacted with *N,N*-dimethylethylenediamine to afford tertiary amine-capped CDs, which are stable without any cross-linking between particles or adjacent surface groups and are, consequently, used as highly photostable and water-soluble photosensitizers in photocatalytic redox processes [40].
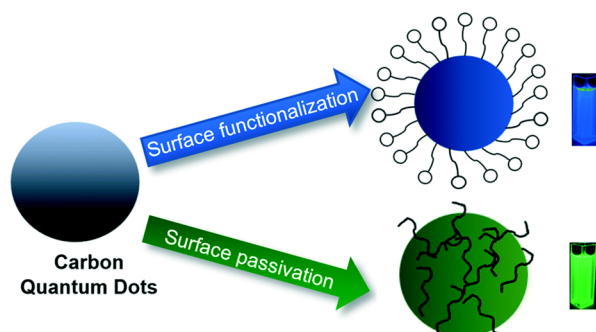
Figure 4. Surface passivation and functionalization of CDs—Reproduced with permission from [29] published by The Royal Society of Chemistry, 2019.

Surface passivation allows one to increase the durability and photostability of CDs by hindering their photocorrosion and minimizing their direct contact with pollutants or reactants. Several non-emissive polymers and organic molecules without chromophores absorbing UV, visible, or near-infrared light are often used as passivation agents, as exemplified by poly(ethylene glycol) diamine with an average molecular weight of 1500 (PEG_{1500N}), poly(propionylethyleneimine-co-ethyleneimine) (PPEI-EI) [41], polyethyleneimine (PEI) [42], and branched polyethyleneimine (BPEI) [43]. A survey of recent research indicates that oligomeric PEG_{1500N}, PPEI-EI, PEI, and BPEI are among the most effective cationic polymer-based passivation agents [44–46], allowing for one to improve fluorescent properties and photostability as well as achieve low toxicity [47]. CDs-PEG_{1500N}, CDs-EI, and CDs-PEI have been used as non-toxic probes for in vitro fluorescent bioimaging and drug delivery in zebrafish [46,48]; however, CDs-BPEI proved to be highly toxic to fish embryos [47]. In the case of surface passivation with PEG_{1500N}, thionyl chloride is widely used as a coupling agent for CD modification [49] (Figure 5A). Moreover, bis(3-aminopropyl)-terminated oligomeric PEG_{1500N} and 2,2′-(ethylenedioxy)bis(ethylamine) (EDA) were efficiently used to passivate the CD surface [50] for fluorescent cell labeling (Figure 5B). The thus synthesized CDs-PEG_{1500N} and CDs-EDA featured relatively high QYs and good stability over a wide pH range [51].
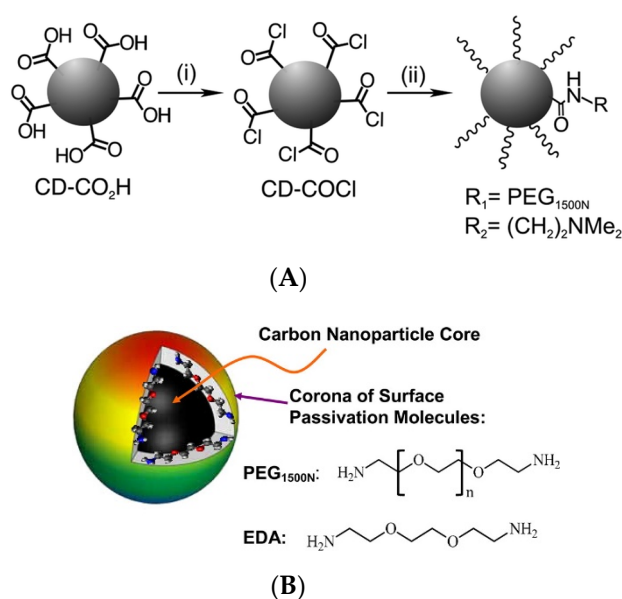

(**A**)

(**B**)

Figure 5. (**A**) Surface passivation of CD containing carboxyl groups (CD-COOH) to CD-COCl using an acyl chloride; (**i**) $SOCl_2$, reflux; (**ii**) addition of alcohol or amine reagents, such as PEG_{1500N} or DMEN—Reproduced with permission from [49] published by The Royal Society of Chemistry, 2017. (**B**) A small carbon nanoparticle core of CDs strongly attached with surface passivated molecules—Reproduced with permission from [50] published by The Royal Society of Chemistry, 2016.

Element doping, e.g., N-doping or dual element doping, can enhance the photocatalytic and luminescent properties of CDs. Nitrogen-doped CDs (N-CDs) exhibit improved photocatalytic activity, as the nitrogen atom has a size that is similar to that of the carbon atom and effectively binds with the latter atoms via five valence electrons [52,53]. Among the photocatalytic applications of N-CDs, one should note those that are related to water treatment and the degradation of organic acids and synthetic dyes [54,55]. N-CDs that are produced via one-pot hydrothermal treatment of cellulose in urea solution [41] exhibit blue-green fluorescence and excitation-dependent emission with QYs of up to 21%. Moreover, the presence of auxochromic nitrogen atoms within the CD architecture results in high QY and promising fluorescent properties. Another work reported the synthesis of sulfur- and nitrogen-co-doped CDs (N,S-CDs), and probed their emission performance under visible-light excitation at 420–520 nm [56]. CDs, N-CDs, S-CDs, and N,S-CDs were prepared by carbonization of citric acid, ethylenediaminetetraacetic acid (EDTA), a mixture of mercaptoacetic and citric acids, and L-cysteine, respectively. Among these CDs, N,S-CDs featured the broadest visible absorption range and the highest absorption intensity in aqueous solution [56].

For CD composite-based photocatalysts, upconverted photoluminescence characteristics for the simultaneous absorption of photons with visible-to-infrared wavelengths (500–1000 nm) and strong emission in the UV-to-visible range (325–425 nm) were observed (Figure 6A). The complexation of CDs with TiO_2 and SiO_2 semiconductors was proposed to extend absorption into the UV range, and TiO_2/CD and SiO_2/CD composites were produced by sol-gel methods [32]. Figure 6B shows scanning electron microscope (SEM) and HR-TEM images of as-synthesized TiO_2/CD and SiO_2/CD photocatalysts, revealing that CDs were attached to the surfaces of TiO_2 or SiO_2 nanoparticles. Regarding the upconverted photoluminescence characteristics of CDs, Figure 6C demonstrates the roles of CDs in photocatalytic pollutant degradation. First, CDs absorb visible light with long wavelengths and then relax by emitting short-wavelength UV photons to induce the photoexcitation of TiO_2 and SiO_2, which results in the generation of electron-hole pairs and liberation of reactive oxygen species (ROS), such as $OH^\bullet$ and $O_2^{\bullet-}$, causing subsequent pollutant degradation. Second, CDs with a proper band gap facilitate electron transfer from the TiO_2 surface after photoexcitation, thus promoting the separation of charges and enhancing the charge transfer for photocatalytic reactions at the photocatalyst surface. Thus, TiO_2/CD and SiO_2/CD photocatalysts facilitate the effective utilization of the full sunlight spectrum.

Li et al. have reported rhree-dimensional (3D) nitrogen-doped carbon dots (N-CDs)/graphene aerogel composites [58]. N-CDs were synthesized from aspartic acid and mixed with graphene oxide solution to form the aerogel composite that was used for the photocatalytic degradation of Cr(VI) under visible light. Later, a 0D/2D CD/g-C_3N_4 composite was investigated as a photocatalyst for sulfamethazine degradation. The 0D/2D heterojunctions of CDs/g-C_3N_4 were synthesized by homogeneous thermal pyrolysis of urea and citric acid as the precursors of g-C_3N_4 and CDs, respectively [59]. A similar one-step homogeneous thermal pyrolysis process that was induced by melting a mixture of citric acid and urea in water was used to synthesize g-C_3N_4-CD photocatalysis for water splitting [60]. Graphitic CDs are commonly produced from citric acid [13,61], while urea typically acts as a crosslinking agent for the polymerization of the g-C_3N_4 network [62,63]. The multiple absorption bands of chemically bonded N-doped CDs were attributed to the $\pi \rightarrow \pi^*$ and $n \rightarrow \pi^*$ transitions of C = C and C = O bonds [64], as well as those of conjugated aromatic C = N bonds [65]. Importantly, the produced CDs featured a good size distribution (1.6–3.0 nm), and the CDs/g-C_3N_4 composite displayed strong photoluminescence at ~540 nm with excitation wavelength–independent emission [60].
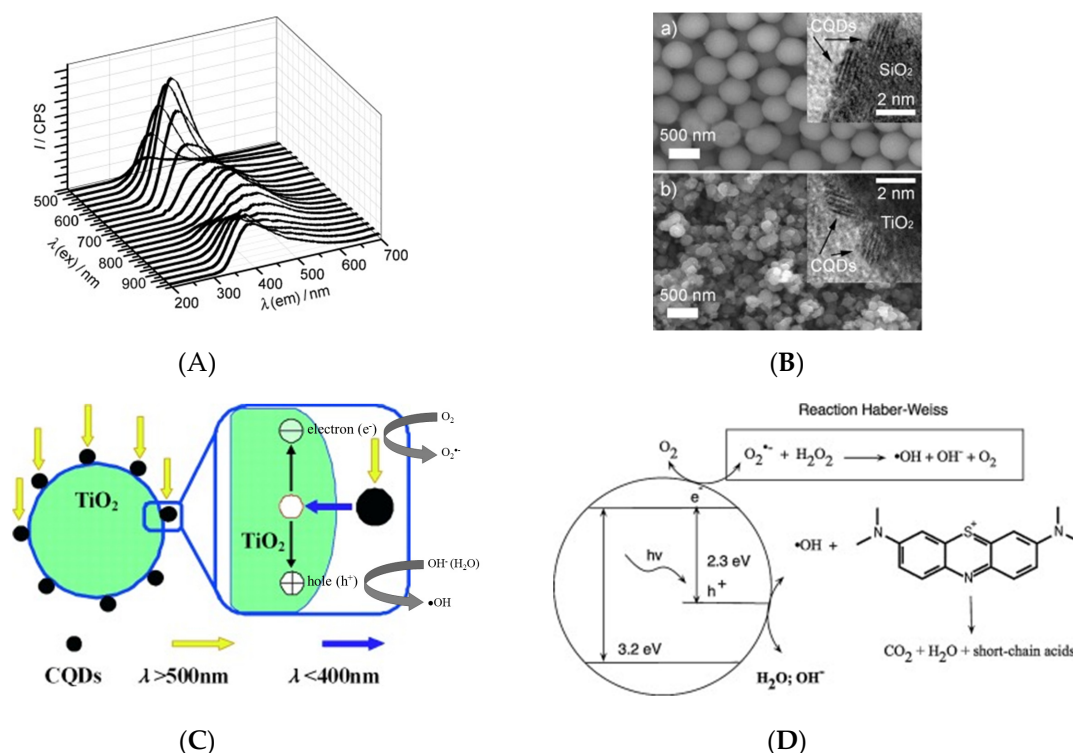
Figure 6. (**A**) Upconversion property on photoluminescence of CDs. (**B**) Scanning electron microscope (SEM) image of SiO$_2$/CDs and TiO$_2$/CDs photocatalysts; Insertion shows the confirming HR-TEM images. (**C**) Photocatalytic mechanism of TiO$_2$/CDs nanocomposite in the range of visible and UV light; Reproduced with permission from [32]. Copyright © 2010 WILEY-VCH Verlag GmbH & Co. KGaA, Weinheim. (**D**) Photocatalytic mineralization of methylene blue; Reproduced with permission from [57] published by Elsevier, 2014.

Metal oxide-decorated CDs have been reported as promising photocatalysts. A facile two-step approach has been used to synthesize CDs that are anchored on TiO$_2$ nanotube arrays (TiO$_2$ NTAs). Electrochemical anodization was performed to prepare TiO$_2$ NTAs, and CDs that were produced by electrolysis of graphite rods were subsequently anchored by electrochemical deposition. The synthesized CDs/TiO$_2$ NTAs acted as a sensitizer to extend the range of light absorption toward the full solar spectrum and, thus, enhance the photocatalytic degradation of pollutants and the efficiency of H$_2$ production via water splitting [66]. CDs that were anchored on an octahedral CoO under hydrothermal conditions also exhibited outstanding performance for photocatalytic water splitting [67]. Moreover, CDs could be fabricated by electrochemical etching of graphite rods, and CD-Fe$_2$O$_3$ nanocomposites that were constructed by facile heat treatment in a tube furnace were found to efficiently catalyze the overall water splitting under visible light in the absence of any external biases or scavengers [68].

The use of composites of transition metal dichalcogenide and CDs in photocatalysis remains underexplored. Zhao et al. [69] hydrothermally synthesized a CDs/MoS$_2$ composite as a catalyst for the hydrogen evolution reaction. CDs that were prepared by electrochemical etching were mixed with MoS$_2$ precursors (Na$_2$MoO$_4$ and L-cysteine) under hydrothermal conditions, and centrifugation then isolated the solid precipitate of CDs/MoS$_2$ containing thin nanosheets (lateral dimension = 50–100 nm). CDs/MoS$_2$ exhibited good catalytic activity for the hydrogen evolution reaction with high cathodic current density and a positive onset over-potential of ~0.109 V. Surprisingly, even better performance was observed when the CD/MoS$_2$ catalyst was exposed to visible light for 30 min. Recently, hybrid CDs/tungsten disulfide quantum dots (CDs/WS$_2$ QDs) have been prepared from sodium tungstate dihydrate and L-cysteine by a bottom-up hydrothermal method and were used as a luminescent probe for the detection of H$_2$O$_2$ and the enzymatic sensing of glucose [70].

Moreover, CDs/WS$_2$ nanorods were found to be suitable for microscopic cell imaging and photothermal therapy. NH$_2$-functionalized WS$_2$ nanorods were mixed with glucose surfactant suspension, followed by thermal treatment to give carbonization CDs that were covalently bound to the WS$_2$ nanorods [71]. Notably, the CDs/WS$_2$ nanorods featured excitation-dependent photoluminescence with a maximum at 430 nm (cf. 450 nm for CDs), which was ascribed to the covalent conjugation of CDs and WS$_2$ nanorods. Similar photoluminescence phenomena were observed for the covalent binding of CDs with other molecules [72].

The photocatalytic applications of CDs have been investigated in a variety of fields, including water treatment, chemical degradation, water splitting, hydrogen evolution, and bio-related applications. The experimental and mechanistic studies on the photocatalytic role of CDs are discussed below.

3.2. Water Treatment and Chemical Degradation

CDs play an important role in photocatalytic water treatment and chemical degradation. During photocatalytic process, electrons (e$^-$) in the photocatalyst are excited by the photon energy and they are promoted from the valence band (VB) to the conduction band (CB). At the same time, the holes (h$^+$) generated in the VB migrates to the surface of photocatalysts, specifically, to the attached CDs as an acceptor of photogenerated holes to prevent electron-hole recombination during photocatalytic processes [29]. Li et al. [32] investigated the photoreduction of methylene blue under visible light that is catalyzed by CD- and nanoparticle-based materials, such as SiO$_2$/CDs, TiO$_2$/CDs, SiO$_2$ nanoparticles, TiO$_2$ nanoparticles, and CDs. The complete degradation of methylene blue was achieved in the presence of SiO$_2$/CDs and TiO$_2$/CDs, while SiO$_2$ nanoparticles, TiO$_2$ nanoparticles, and CDs had no effect on methylene blue degradation. Therefore, CDs were concluded to be essential for visible-light photodegradation, as pure SiO$_2$ and TiO$_2$ were completely inactive. Figure 6C explains the mechanistic role of CDs in photodegradation [32]. When the TiO$_2$/CDs or SiO$_2$/CDs photocatalyst is photoilluminated, the CDs absorb visible light, and then emit shorter wavelength light (325 to 425 nm), which in turn excites TiO$_2$ or SiO$_2$ to form electron/hole (e$^-$/h$^+$) pairs. The electron/hole pairs then react with the adsorbed oxidants/reducers (usually O$_2$/OH$^-$) to produce active oxygen radicals (e.g., ·O$_2^-$, ·OH), which subsequently cause the degradation of the methylene blue dyes, as illustrated in Figure 6D [57]. Promising photocatalytic activity for rhodamine B degradation was achieved by sulfur and nitrogen co-doped CDs(N,S-CDs)/TiO$_2$ composites under excitation at 420–520 nm [54]. N,S-CDs also achieved the rapid mineralization of nitrophenols under visible light [56]. A CD model consisting of 42 carbon atoms, 18 hydrogen atoms, and 1 oxygen atom (C$_{42}$H$_{18}$O) was used to study the electronic structure of the undoped CDs. The doping of CDs with one sulfur atom (C$_{40}$H$_{16}$OS) decreased the band gap from 3.440 to 3.247 eV, while doping with two nitrogen atoms (C$_{39}$H$_{16}$ON$_2$) decreased the band gap to 3.234 eV. Interestingly, the band gap of N,S-CDs was further reduced to 3.103 eV, which indicates that nitrogen and sulfur co-doping was most effective in reducing the band gap, mainly because heteroatom doping results in the charge redistribution of doped CDs [73].

The achieved Cr(VI) degradation efficiency (90.6%) exceeded those that were obtained for CD/GA composite without N-doping and N-CDs without the graphene aerogel when visible light ($\lambda > 420$ nm)-driven water remediation was catalyzed by 3D N-CD/graphene aerogel (N-CD/GA) composites [57]. During the catalytic degradation of Cr(VI), potassium dichromate (K$_2$Cr$_2$O$_7$) was used as a model compound and, due to the presence of triethanolamine as a sacrificial agent, CrO$_4^{2-}$ anion is the main chemical form of Cr (VI) in alkaline solutions. The photocatalytic reduction of Cr(VI) can be expressed as CrO$_4^{2-}$ + 8H$^+$ + 3e^- = Cr^{3+} + 4H$_2$O. Under visible-light irradiation, the electrons in the HOMO of N-CDs are excited to the LUMO, which leaves the former orbital with holes that can oxidize triethanolamine as an electron donor. The photogenerated electrons on N-CDs migrate to the surface of the graphene aerogel and then reduce toxic Cr(VI) to nontoxic Cr(III).

Despite its promising photophysical and electronic properties, graphitic carbon nitride (g-C$_3$N$_4$) only exhibits moderate photocatalytic performance [74,75]. Most recently, a 0D/2D CD/g-C$_3$N$_4$ composite has been investigated in terms of photocatalytic activity for the degradation of sulfamethazine

(SMZ) under irradiation with LED light (380–780 nm) [59]. CDs/g-C_3N_4 (CDCNs) were denoted as CDCN-n, where n is the initial mass of citric acid as a precursor for the synthesis of CDs [59]. CDCN-10 presented the highest photocatalytic performance, achieving an approximately 90% degradation under irradiation with LED (420–500 nm) light or Xe lamp (380–780 nm). Specifically, to completely degrade SMZ, the energy consumption of LED (ca. 50 Wh) was estimated to be ca. 15 times less than that of Xe lamp (ca. 750 Wh). Therefore, LED was more effective than Xe lamps in terms of decomposing SMZ and energy consumption. The Mott–Schottky plots were applied and considered as the conduction-band energy (ECB) to further clarify the effects of CDs on the band structure of CDs/g-C_3N_4. Figure 7A shows that the conduction-band energy from the Mott–Schottky plots of g-C_3N_4 and CDCN-10 at −1.42 and −1.28 eV, respectively. Moreover, electrochemical impedance spectroscopy was used to elucidate the photosemiconductor charge generation, migration, and separation behaviors, and the curvature radius of the corresponding Nyquist plot was indicative of electron transfer resistance [76]. The results revealed that the charge transfer resistance of g-C_3N_4 substantially exceeded that of CDs/g-C_3N_4 (Figure 7B), which implied that CDs accelerated charge transfer during photocatalysis. The generated electrons also partially reacted with dissolved oxygen to form $O_2^{\bullet-}$, as the standard redox potential of $O_2/O_2^{\bullet-}$ (−0.33 eV) is less negative than the conduction-band potential of CDs/g-C_3N_4 (−1.28 eV). Other ROS, such as $OH^\bullet$, $^1O_2$, and H_2O_2, could also be generated to assist the degradation of sulfamethazine due to the $O_2^{\bullet-}$ transformation [59] (Figure 7C).
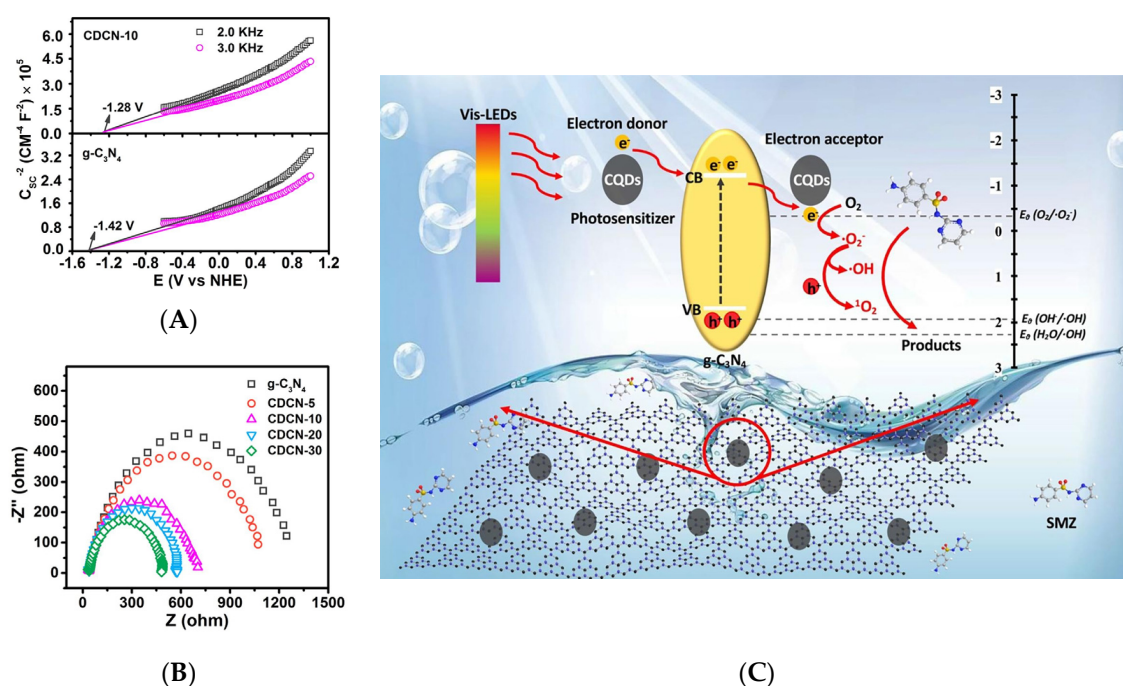

Figure 7. (**A**) Mott–Schottky plots. (**B**) Electrochemical impedance spectroscopy of g-C_3N_4 and CDs/g-C_3N_4. (**C**) Photocatalytic mechanism of sulfamethazine catalyzed by CDs/g-C_3N_4 under visible LED irradiation; Reprinted with permission from [59] published by Elsevier, 2020.

Most recently, a study revealed the effect of precursors and synthesis methods on CDs characteristics and their photoinduced electron transfer (PET) reactivity for single electron photoreduction of methyl viologen MV^{2+} (−0.45 V vs. NHE) to its mono-reduced species ($MV^{\bullet+}$). The synthesis of CDs from all glucose, fructose, and citric acid using hydrothermal synthesis yielded low density and amorphous CDs, while that using pyrolysis rendered graphitic structures. Citric acid-derived CDs were the most photoactive nano-systems, followed by fructose and glucose analogues. Graphitic CDs from citric acid and glucose facilitated higher performance on photoreduction of MV^{2+} when compared with amorphous CDs. However, the contradict results of amorphous CDs were found for fructose precursor. The reason for this inversion was possibly due to the formation of the supramolecular aggregates from

large graphitic materials, which affects the PET efficiency [77]. Another work additionally disclosed that the hydrothermal syntheses yielded amorphous CDs from citric acid, which were either nondoped (a-CDs) or nitrogen-doped (a-N-CDs), whereas the pyrolytic treatment afforded graphitic CDs, either non-doped (g-CDs) or nitrogen-doped (g-N-CDs) [78]. For non-nitrogen-doped CDs, graphitic CDs works utmost in the photoreduction of MV^{2+} relative to amorphous CDs, nevertheless amorphous nitrogen-doped CDs are greater active when compared to their graphitic N-CDs.

Briefly, CDs can significantly improve the efficiency of photocatalytic water treatment and chemical degradation in view of their upconversion properties and the promotional effect on charge transfer to suppress electron-hole recombination. However, the role of surface chemistry of CDs in the induction of charge photogeneration needs to be further clarified.

3.3. Water Splitting and Hydrogen Evolution

Hydrogen production by solar-energy-driven water splitting has been extensively studied as a means of green mass production of hydrogen to cover future energy demand. During photocatalytic water splitting, water is decomposed into hydrogen and oxygen according to eq. (1) (Figure 8).
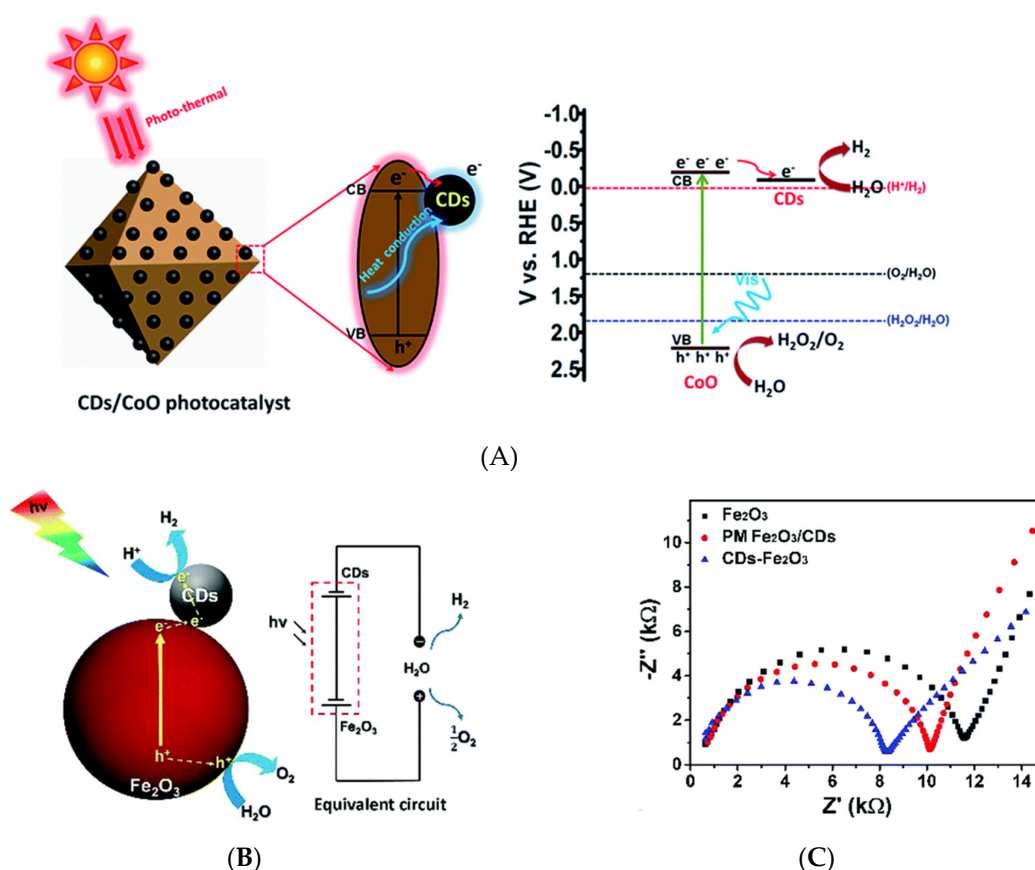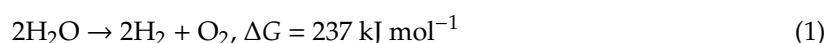
$$2H_2O \rightarrow 2H_2 + O_2, \Delta G = 237 \text{ kJ mol}^{-1} \tag{1}$$

Figure 8. (**A**) The mechanism of visible-light driven water splitting by carbon dots decorated on octahedral CoO surface- Reproduced with permission from [67]—published by The Royal Society of Chemistry, 2017. (**B**) Water splitting mechanism of CDs/Fe_2O_3 under visible light and the equivalent circuit, and (**C**) Electrochemical impedance spectra of Fe_2O_3, physically mixed CDs and Fe_2O_3 (PM Fe_2O_3/CDs), and CDs/Fe_2O_3—Reproduced with permission from [68] published by The Royal Society of Chemistry, 2018.

Recent reviews have summarized the influence of CDs on the efficiency of photocatalytic water splitting for hydrogen production [79,80]. A recent work on the role of graphitic CDs that are anchored on TiO_2 nanotube arrays (TiO_2 NTAs) in photocatalytic water splitting [66] showed that CDs in CDs/TiO_2 NTAs act as a sensitizer for extending the light absorption range toward the full solar spectrum. Electrochemical impedance spectroscopy was used to analyze electron-hole pair separation and transfer under light irradiation, revealing that CDs strongly reduced charge transfer resistance. Photoelectrochemical tests that were performed at various deposition times showed that the photoelectron density generated by CDs/TiO_2 NTAs exceeded that generated by pristine TiO_2 NTAs. The former composite additionally featured an extended absorption spectrum spanning both visible and near-infrared (NIR) ranges [66]. Optimal photocatalytic water splitting under visible-light irradiation ($\lambda > 400$ nm) was achieved while using a CD/CoO composite as a photocatalyst, with the observed hydrogen and oxygen evolution rates (1.67 and 0.91 μmol h^{-1}, respectively) corresponding to the expected 2:1 stoichiometry. These production rates were up to six-fold higher than those of pristine CoO. The photogenerated electrons in the conduction band of CoO spontaneously migrated to CDs for hydrogen evolution, owing to the effect of CDs on electron transfer, as illustrated in Figure 8A. This migration suppressed the recombination of electron-hole pairs and, thus, increased the photocatalytic activity of CoO. In addition, CDs can act as a heat conductor for dissipating the heat accumulated because of the photothermal effect at the surface of CoO and, thus, prevent its deactivation [67]. The CDs/Fe_2O_3 composite can be also used for a water splitting catalyst. CDs were found to decrease the separation between the hematite (Fe_2O_3) conduction band and H^+/H_2 potential. The ionization potential that was equivalent to the valence band energy (E_V) of CDs/Fe_2O_3 was measured by ultraviolet photoelectron spectroscopy (UPS). The E_V value is determined to be 6.29 eV by subtracting the width of the He I UPS spectrum from the exciting energy (21.22 eV). The Ev value from UPS measurement is consistent with that from electrochemistry while using cyclic voltammetry of CDs/Fe_2O_3, which can be used to investigate the highest occupied molecular orbital (HOMO) and the lowest unoccupied molecular orbital (LUMO) of CDs/Fe_2O_3 using the ferrocene redox system as the external standard. E_{HOMO} and E_{LUMO} were calculated from $E_{HOMO} = -(Eox_{onset} - E_{ferrocene} + 4.8)$ eV and $E_{LUMO} = -(E^{red}_{onset} - E_{ferrocene} + 4.8)$ eV, respectively, where E^{ox}_{onset}, E^{red}_{onset}, and $E_{ferrocene}$ are the onset of oxidation and reduction potential of CDs/Fe_2O_3 and the oxidation potential of ferrocene, respectively. The calculated HOMO/LUMO energy levels are $-6.255/-4.233$ eV for CDs/Fe_2O_3 corresponding to the bandgap of 2.02 eV for CDs/Fe_2O_3, while the bandgap of Fe_2O_3 was reported to be 2.1 eV [68]. CDs/Fe_2O_3 nanocomposites with 5 wt% CDs effectively promoted photocatalytic water splitting under visible-light irradiation in the absence of scavengers or external bias, affording hydrogen and oxygen at rates of 0.390 and 0.225 μmol h^{-1}, respectively. Figure 8B illustrates the visible-light absorption of Fe_2O_3 ($\lambda \geq 420$ nm) and the generation of electron-hole pairs upon visible-light irradiation. The holes directly reacted with water to produce O_2, while the photogenerated electrons were transferred from the conduction band of Fe_2O_3 to CDs for hydrogen evolution. Finally, CDs additionally improved the light absorption of Fe_2O_3 and enhanced the charge separation ability, as evidenced by the reduced resistance [68] (Figure 8C).

Wang et al. [81] designed a hybrid photocatalyst containing inner CDs that were attached to outer layer of single-layer carbon nitride (C_3N) to control the reduction and oxidation sites during water splitting. C_3N is a graphene-like planar hexagonal structure with the nitrogen being uniformly distributed. The geometric and electronic structures of C_3N were studied with density functional theory (DFT) prior to combination with CDs. The simulations suggested that this hybrid material can harvest the entire visible and infrared light for water splitting. Upon irradiation with visible light, free electrons and holes are formed in the hybrid CD-C_3N composite, with electrons accumulating in the inner CDs and the holes accumulating on the outer C_3N layer. Holes at the C_3N oxidation sites attack the adsorbed water molecules and promote their splitting to generate protons, which penetrate C_3N due to the low barrier of 2.30 eV based on the concentration gradient and electrostatic attraction. In contrast, oxygen-containing products cannot penetrate the above layer because of the

high penetration barrier of 6.28 eV. After migration, protons combine with electrons on CD reduction sites to generate H_2. As only protons and H atoms penetrate C_3N, the produced H_2 is stored in the C_3N layer and separated from oxygen species [81]. Thus, the above hybrid is a promising material for photocatalytic water splitting.

The difficulty of overall water splitting for hydrogen and oxygen production lies in the control of the reduction and oxidation sites, which should be located within a close distance in the same photocatalyst. Therefore, the reverse reaction and even explosion can occur when the hydrogen and oxygen that are produced in/on a photocatalyst are combined. Metal-free hybrid materials are attractive photocatalysts for the practical conversion of solar energy and the generation/utilization of hydrogen in view of their well-separated reduction-oxidation characteristics. However, experimental evidence is needed to confirm the theoretical assumption that is based on molecular simulations.

4. Enzyme-Mimetic and Photodynamic Applications

CDs exhibit outstanding electrochemiluminescent properties, similar to semiconductor QDs, which, together with their high biocompatibility, low toxicity, easy synthesis, high chemical inertness, excitation-dependent multicolor emission, and photobleaching resistance, make CDs attractive for bio-related applications. Herein, we focus on the nanozyme and photodynamic applications of CDs.

Natural photosynthesis has inspired the use of synthetic enzymes in photocatalysis. In particular, the remarkable water dispersibility of CDs, attributed to their abundant hydrophilic groups introduced by surface engineering, makes them promising nanomaterials for nanozyme applications. Recent research has uncovered the important role of peroxidases (POD) as drivers of angiogenesis, which is related to tumor growth [82]. CDs were shown to exhibit POD-like activity in the presence of H_2O_2, as evaluated by the color of oxidized chromogenic substrates [83], e.g., *o*-phenylenediamine (OPD), hydroquinone, 1,2,3-trihydroxybenzene (THB), and 3,3′,5,5′-tetramethylbenzidine (TMB). Among them, TMB is the most widely used substrate for investigating POD- and horseradish peroxidase (HRP)-mimetic activity of nanozymes due to its low carcinogenicity and strong absorbance [84–86]. Shi et al. [87] discovered that candle soot–derived CDs exhibit POD-like catalytic activity for THB, OPD, and TMB oxidation in the presence of H_2O_2. The developed color indicates the quantity of oxidized TMB, as illustrated in Figure 9. In contrast to HRP, CDs exhibit very stable catalytic activity over a broad temperature range (0–90 °C) and a wide pH range (pH 2–12). Moreover, the catalytic mechanism of CDs, which is based on a ping-pong model, is similar to that of HRP, with CDs having a higher affinity to POD substrates and H_2O_2 [87]. The combination of POD-mimetic CDs with glucose oxidase (GOx) was shown to provide a cheap, simple, selective, and sensitive assay for colorimetric glucose sensing in serum [87].
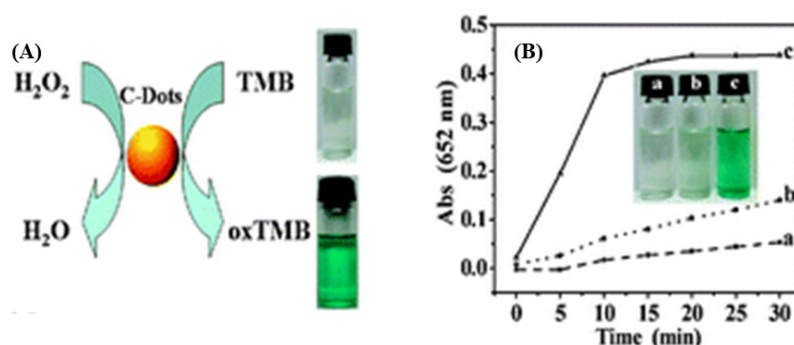

Figure 9. (**A**) Schematic illustration, and (**B**) Time-dependent absorbance of oxidized TMB by CDs at 652 nm in different systems: (**a**) TMB+CDs, (**b**) TMB + H_2O_2, and (**c**) TMB + CDs + H_2O_2—Reproduced with permission from [87] published by The Royal Society of Chemistry, 2011.

Recent years have witnessed significant progress in the application of CDs as photosensitizers and photodriven nanozymes [40,88,89]. Hutton et al. [40] reported light-driven enzymatic catalysis by CDs for a

system of simultaneous hydrogenation and hydrogen production. Positively charged ammonium-doped CDs (CD-NHMe$_2^+$) allowed for the photoexcited electrons to be transferred to negatively charged fumarate reductase (FccA) for the reduction of fumarate to succinate via hydrogenation with a turnover number of 6,000 mol succinate per mol FccA within 24 h, as demonstrated for system A in Figure 10A. Simultaneously, CD-NHMe$_2^+$ could enhance solar hydrogen generation by transferring photogenerated electrons to [NiFeSe]-hydrogenase (H$_2$ase) for hydrogen production via proton reduction with turnover numbers of 43,000 mol H$_2$ per mol H$_2$ase in 24 h, as demonstrated for system B in Figure 10A. In contrast, negatively charged CDs with carboxyl groups (CD-COO$^-$) exhibited little or no effect on both of the reactions [40]. Lin et al. [88] designed a CD-based dual optical and photoelectrochemical immunosensing system for monitoring aflatoxin B1 (AFB$_1$) in food, which achieved highly selective AFB$_1$ detection in a magneto-controlled immunoreaction system (Figure 10B). GOx delivered on the tag oxidized glucose to gluconic acid and H$_2$O$_2$ once the immunocomplexes of GOx-labeled bovine serum albumin-AFB$_1$ were formed. Subsequently, MnO$_2$ nanosheets on the MnO$_2$-CD–coated electrode reacted with H$_2$O$_2$ to induce the dissociation of CDs and photocurrent decline. The detection of AFB$_1$ was achieved in the range of 0.01–20 ng mL^{-1}, with a detection limit of 2.1 pg mL^{-1} (ppt) [88]. The established immunoassay demonstrated satisfactory accuracy and good reproducibility. Zhang et al. [89] used phosphorescent CDs as a photo-oxidative nanozyme for antimicrobial photodynamic inactivation, achieving 92 and 86% growth inhibition efficiencies against *Escherichia coli* and *Salmonella* under light irradiation, respectively. In contrast, phloxine B, which is a commercial photosensitizer, displayed inhibition efficiencies of only 40 and 55%, respectively. Figure 10C(a) illustrates the photodriven activation of oxygen on the photosensitizer to produce singlet oxygen from triplet O$_2$, which is the cheapest, most abundant, and environmentally friendly oxidant. Promising photosensitizers facilitate the transition of fluorescence to phosphorescence with a high yield of the triple state, and the photosensitization efficiency is proportional to phosphorescence (Figure 10C(b)). CDs exhibited the activity of an oxidase-mimicking nanozyme, as confirmed by the strong absorbance at ~652 nm, due to the photo-oxidation of TMB (Figure 10C(c)). Similarly, a CD/polydimethylsiloxane composite was reported to exhibit photodynamic antibacterial activity against *E. coli*, *Staphylococcus aureus*, and *Klebsiella pneumonia* under blue-light irradiation for only 15 min. [90].
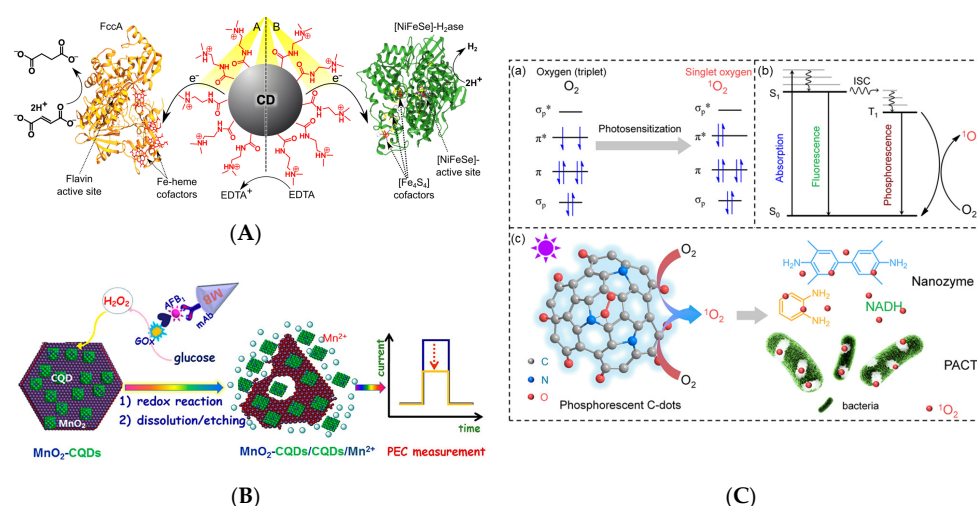

Figure 10. (**A**) Light-driven photocatalytic hydrogenation of fumarate to succinate and hydrogen generation by CD-NHMe$_2^+$; Reprinted with permission from [40]. Copyright © 2016, American Chemical Society. (**B**) Aflatoxin B$_1$ (AFB$_1$) detection using photoelectrochemical immunosensing assay by CDs-coated MnO$_2$ nanosheets; Reprinted with permission from [88]. Copyright © 2017, American Chemical Society. (**C**) Photo-activation of oxygen by CDs: (**a**) oxygen photosensitization, (**b**) phosphorescence Jablonski energy chart of singlet oxygen, and (**c**) photosensitized oxygen activated antimicrobial activity of CDs; Reprinted with permission from [89]. Copyright © 2018, American Chemical Society.

To sum up, the photoresponsive characteristics and efficient endorsement of redox enzyme activity of CDs allow for them to be used in numerous enzyme-driven reactions (e.g., hydrogenation and hydrogen evolution). Moreover, the exceptional photosensitization behavior of CDs for singlet oxygen generation can be used in photodynamic therapy, which broadens the research scope for CD utilization in photobiocatalysis. Nevertheless, to more precisely realize controllable reactions, one should further investigate suitable chemical modifications of the CD surface, allowing for resistance toward photodegradation and increased stability during photodriven reactions.

5. Summary and Future Prospects

CD research, development, and applications have recently drawn significant attention. The ability of functionalized CDs to absorb in the entire solar spectrum range, from ultraviolet to NIR, makes them outstanding materials for multi-disciplinary research in the fields of photocatalysis, photoelectrocatalysis, and optoelectronics. Photoluminescence is another fascinating optical feature of CDs regarding their emission ability due to their tunable, photoresponsive characteristics. Besides, the upconverted photoluminescent behavior of CDs, which can efficiently absorb at multiple wavelengths and emit relatively short-wavelength light, potentially expands their benefits to the advanced progress of fabricating various remarkable photodevices. When combined with low toxicity and biocompatibility, the photoresponsive behavior of CDs expands their application scope to the area of bio-related research, including enzyme-mimetic and photodynamic applications. However, we do not deal with other bio-applications, such as biosensing, bioimaging, and phototheranostics, in this review because they are not related to catalysis.

Currently, the main challenges of CD research and development are the limited potential for commercialization and the determination of the most suitable modification for target applications. Conventionally, top-down methods of CDs synthesis, such as laser ablation, ultrasonication, and electrochemical etching of graphite or carbon materials, have been used. Recently, scalable bottom-up methods of CD synthesis from carbon-containing molecules, including carbohydrates, organic acids, and natural products, have been developed to accurately control CD morphology and size for large-scale production. Moreover, in the case of bottom-up approaches, the synthesis and surface modification of CDs can be performed in a single step. Most CD synthesis techniques feature hydrothermal treatment, chemical treatment, microwave synthesis, solvothermal treatment, and plasma treatment, and are, therefore, challenging to integrate with the thermochemical conversion of biomass to fuels and bio-crudes, which are carbon-rich materials.

To obtain CDs with tunable and distinctive optical and photoluminescent characteristics, one should control their size and surface modification. After synthesis, downstream processing and purification of CDs are crucial, as the low density and surface charge of CDs make them difficult to separate by normal centrifugation. Most of the researchers applied dialysis and gel chromatography techniques to isolate CDs with a particular size. Recent works have additionally paid attention to the surface modification of CDs by functionalization with amine, carboxyl, hydroxyl, and carbonyl groups or specific molecules, passivation with polymers or organic molecules, non-metal or metal doping, and composite formation with one-dimensional/two-dimensional (1D/2D) materials.

In the case of photocatalytic applications, pure CDs cannot be used as photocatalysts or photosensitizers. However, CD composites with other photocatalysts or semiconductors can absorb photons with energy that is equal to or greater than the band gap. CDs can enhance the photocatalytic activity of these materials in two ways. First, CDs absorb long-wavelength visible light and then relax by emitting photons in the short-wavelength UV range to photoexcite semiconductor photocatalysts. Second, CDs with a proper band gap further assist photogenerated electron transfer from the surface of semiconductor photocatalysts after photoexcitation, which promotes the separation of charges and enhances charge migration efficiency by increasing the number of charge carriers that are available for photocatalytic reactions. In view of the upconverted photoluminescent properties of CDs, composites of CDs with other photocatalysts/semiconductors facilitate the effective exploitation of the whole

sunlight spectrum. Consequently, the applications of CDs for light-induced catalysis, including energy conversion and storage, water splitting, hydrogen evolution, water treatment, chemical degradation, and their bio-related applications have significantly expanded in recent years. In particular, the surface modification of bio-derived CDs for enzyme-mimetic reactions, bioimaging, targeted drug delivery, and phototheranostics is a promising trend for CD applications. The surface modification of CDs to attain high solubility in aqueous media and good photostability affords versatile photosensitizers for promoting redox enzyme activity, which additionally broadens the research scope for CD utilization in photobiocatalysis.

References Critical

1. Qu, S.; Wang, X.; Lu, Q.; Liu, X.; Wang, L. A biocompatible fluorescent ink based on water-soluble luminescent carbon nanodots. *Angew. Chem. Int. Ed.* **2012**, *51*, 12215–12218. [CrossRef]

2. Zhang, J.; Yu, S.H. Carbon dots: Large-scale synthesis, sensing and bioimaging. *Mater. Today* **2016**, *19*, 382–393. [CrossRef]

3. Wang, J.; Wang, C.F.; Chen, S. Amphiphilic egg-derived carbon dots: Rapid plasma fabrication, pyrolysis process, and multicolor printing patterns. *Angew. Chem. Int. Ed.* **2012**, *51*, 9297–9301. [CrossRef] [PubMed]

4. Xu, X.; Ray, R.; Gu, Y.; Ploehn, H.J.; Gearheart, L.; Raker, K.; Scrivens, W.A. Electrophoretic analysis and purification of fluorescent single-walled carbon nanotube fragments. *J. Am. Chem. Soc.* **2004**, *126*, 12736–12737. [CrossRef] [PubMed]

5. Shen, J.; Zhu, Y.; Yang, X.; Li, C. Graphene quantum dots: Emergent nanolights for bioimaging, sensors, catalysis and photovoltaic devices. *Chem. Commun.* **2012**, *48*, 3686–3699. [CrossRef] [PubMed]

6. Li, L.; Wu, G.; Yang, G.; Peng, J.; Zhao, J.; Zhu, J.J. Focusing on luminescent graphene quantum dots: Current status and future perspectives. *Nanoscale* **2013**, *5*, 4015–4039. [CrossRef]

7. Tuerhong, M.; Xu, Y.; Yin, X.B. Review on carbon dots and their applications. *Chin. J. Anal. Chem.* **2017**, *45*, 139–150. [CrossRef]

8. Zhang, L.; Wang, Y.; Liu, W.; Ni, Y.; Hou, Q. Corncob residues as carbon quantum dots sources and their application in detection of metal ions. *Ind. Crop. Prod.* **2019**, *133*, 18–25. [CrossRef]

9. Yang, C.; Thomsen, R.P.; Ogaki, R.; Kjems, J.; Teo, B.M. Ultrastable green fluorescence carbon dots with a high quantum yield for bioimaging and use as theranostic carriers. *J. Mater. Chem. B* **2015**, *3*, 4577–4584. [CrossRef]

10. Ana, J.C.S.; Camacho, D.H. Influence of precursor size in the hydrothermal synthesis of cellulose-based carbon nanodots and its application towards solar cell sensitization. *Mater. Chem. Phys.* **2019**, *228*, 187–193. [CrossRef]

11. Su, H.; Bi, Z.; Ni, Y.; Yan, L. One-pot degradation of cellulose into carbon dots and organic acids in its homogeneous aqueous solution. *Green Energy Environ.* **2019**, *4*, 391–399. [CrossRef]

12. Yuan, Y.; Guo, B.; Hao, L.; Liu, N.; Lin, Y.; Guo, W.; Li, X.; Gu, B. Doxorubicin-loaded environmentally friendly carbon dots as a novel drug delivery system for nucleus targeted cancer therapy. *Colloids Surf. B* **2017**, *159*, 349–359. [CrossRef]

13. Ludmerczki, R.; Mura, S.; Carbonara, C.M.; Mandity, M.M.; Carraro, M.; Senes, N.; Garroni, S.; Granozzi, G.; Calvillo, L.; Marras, S.; et al. Carbon dots from citric acid and its intermediates formed by thermal decomposition. *Chem. Eur. J.* **2019**, *25*, 11963–11974. [CrossRef]

14. Zhang, J.; Liu, X.; Zhou, J.; Huang, X.; Xie, D.; Ni, J.; Ni, C. Carbon dots derived from algae as H_2O_2 sensors: The importance of nutrients in biomass. *Nanoscale Adv.* **2019**, *1*, 2151–2156. [CrossRef]

15. Sharma, A.; Das, J. Small molecules derived carbon dots: Synthesis and applications in sensing, catalysis, imaging, and biomedicine. *J. Nanobiotechnol.* **2019**, *17*, 92. [CrossRef] [PubMed]

16. Liu, H.; Li, Z.; Sun, Y.; Geng, X.; Hu, Y.; Meng, H.; Ge, J.; Qu, L. Synthesis of luminescent carbon dots with ultrahigh quantum yield and inherent folate receptor-positive cancer cell targetability. *Sci. Rep.* **2018**, *8*, 1086. [CrossRef] [PubMed]

17. Khan, Z.M.S.H.; Rahman, R.S.; Islam, S.; Zulfequar, M. Hydrothermal treatment of red lentils for the synthesis of fluorescent carbon quantum dots and its application for sensing Fe^{3+}. *Opt. Mater.* **2019**, *91*, 386–395. [CrossRef]

18. Rai, S.; Singh, B.K.; Bhartiya, P.; Singh, A.; Kumar, H.; Dutta, P.K.; Mehrotra, G.K. Lignin derived reduced fluorescence carbon dots with theranostic approaches: Nano-drug-carrier and bioimaging. *J. Lumin.* **2017**, *190*, 492–503. [CrossRef]

19. Yang, X.; Yang, X.; Li, Z.; Li, S.; Han, Y.; Chen, Y.; Bu, X.; Su, C.; Xu, H.; Jiang, Y.; et al. Photoluminescent carbon dots synthesized by microwave treatment for selective image of cancer cells. *J. Colloid Interface Sci.* **2015**, *456*. [CrossRef]

20. Wang, T.Y.; Chen, C.Y.; Wang, C.M.; Tan, Y.Z.; Liao, W.S. Multicolor functional carbon dots via one-step refluxing synthesis. *ACS Sens.* **2017**, *2*, 354–363. [CrossRef]

21. da Silva Souza, D.R.; Caminhas, L.D.; de Mesquita, J.P.; Pereira, F.V. Luminescent carbon dots obtained from cellulose. *Mater. Chem. Phys.* **2018**, *203*, 148–155. [CrossRef]

22. Jiao, X.-Y.; Li, L.S.; Qin, S.; Zhang, Y.; Huang, K.; Xu, L. The synthesis of fluorescent carbon dots from mango peel and their multiple applications. *Colloids Surf. A Physicochem. Eng. Asp.* **2019**, *577*, 306–314. [CrossRef]

23. Niu, F.; Xu, Y.; Liu, M.; Sun, J.; Guo, P.; Liu, J. Bottom-up electrochemical preparation of solid-state carbon nanodots directly from nitriles/ionic liquids using carbon-free electrodes and the applications in specific ferric ion detection and cell imaging. *Nanoscale* **2016**, *8*, 5470–5477. [CrossRef] [PubMed]

24. Allam, A.; Sarkar, S. Water Soluble Fluorescent Quantum Carbon Dots. U.S. Patent 8,357,507, 22 January 2013.

25. Yao, J.; Gao, J.; Shen, P. Synthesis Method for Preparing Water-Soluble Biomass-Based Fluorescent Carbon Dot and Application. CN 105314621A, 10 February 2016.

26. Wang, D.; Pu, Y.; Chen, J. Biomass Nitrogen Doped Fluorescent Carbon Dot Preparation Method. CN 106318390A, 4 January 2019.

27. Zhang, S.; Chen, H.; Kay, C.; Su, K.; Zhou, Y.; Wang, Q. Biomass-Based Carbon Quantum Dot and Preparation Method Thereof. CN 107418567A, 1 December 2017.

28. Yuan, H.; Li, D.; Zhang, X. Preparation Method of Biomass Tar Derived Carbon Quantum Dot. CN 107722974A, 15 January 2019.

29. Phang, S.J.; Tan, L.L. Recent advances in carbon quantum dots (CQDs)-based two dimensional materials for photocatalytic applications. *Catal. Sci. Technol.* **2019**, *9*, 5882–5905. [CrossRef]

30. Colmenares, J.C.; Luque, R. Heterogeneous photocatalytic nanomaterials: Prospects and challenges in selective transformations of biomass-derived compounds. *Chem. Soc. Rev.* **2014**, *43*, 765–778. [CrossRef]

31. Konstantinos, D. Carbon quantum dots: Surface passivation and functionalization. *Curr. Org. Chem.* **2016**, *20*, 682–695. [CrossRef]

32. Li, H.; He, X.; Kang, Z.; Huang, H.; Liu, Y.; Liu, J.; Lian, S.; Tsang, C.H.A.; Yang, X.; Lee, S.-T. Water-soluble fluorescent carbon quantum dots and photocatalyst design. *Angew. Chem. Int. Ed.* **2010**, *49*, 4430–4434. [CrossRef]

33. Shi, Y.; Pan, Y.; Zhong, J.; Yang, J.; Zheng, J.; Cheng, J.; Song, R.; Yi, C. Facile synthesis of gadolinium (III) chelates functionalized carbon quantum dots for fluorescence and magnetic resonance dual-modal bioimaging. *Carbon* **2015**, *93*, 742–750. [CrossRef]

34. Malfatti, L.; Innocenzi, P. Sol-gel chemistry for carbon dots. *Chem. Rec.* **2018**, *18*, 1192–1202. [CrossRef]

35. Yan, F.; Jiang, Y.; Sun, X.; Bai, Z.; Zhang, Y.; Zhou, X. Surface modification and chemical functionalization of carbon dots: A review. *Microchim. Acta* **2018**, *185*, 424. [CrossRef]

36. Tachi, S.; Morita, H.; Takahashi, M.; Okabayashi, Y.; Hosokai, T.; Sugai, T.; Kuwahara, S. Quantum yield enhancement in graphene quantum dots via esterification with benzyl alcohol. *Sci. Rep.* **2019**, *9*, 14115. [CrossRef] [PubMed]

37. Guo, C.X.; Zhao, D.; Zhao, Q.; Wang, P.; Lu, X. Na⁺-functionalized carbon quantum dots: A new draw solute in forward osmosis for seawater desalination. *Chem. Commun.* **2014**, *50*, 7318–7321. [CrossRef] [PubMed]

38. Martindale, B.C.M.; Hutton, G.A.M.; Caputo, C.A.; Reisner, E. Solar hydrogen production using carbon quantum dots and a molecular nickel catalyst. *J. Am. Chem. Soc.* **2015**, *137*, 6018–6025. [CrossRef] [PubMed]

39. Liu, C.; Bao, L.; Tang, B.; Zhao, J.Y.; Zhang, Z.L.; Xiong, L.H.; Hu, J.; Wu, L.L.; Pang, D.W. Fluorescence-converging carbon nanodots-hybridized silica nanosphere. *Small* **2016**, *12*, 4702–4706. [CrossRef]

40. Hutton, G.A.M.; Reuillard, B.; Martindale, B.C.M.; Caputo, C.A.; Lockwood, C.W.J.; Butt, J.N.; Reisner, E. Carbon dots as versatile photosensitizers for solar-driven catalysis with redox enzymes. *J. Am. Chem. Soc.* **2016**, *138*, 16722–16730. [CrossRef]

41. Zhao, P.; Zhu, L. Dispersibility of carbon dots in aqueous and/or organic solvents. *Chem. Commun.* **2018**, *54*, 5401–5406. [CrossRef]

42. Peilian, S.; Junkuo, G.; Jingkun, C.; Ziwei, L.; Changqing, L.; Juming, Y. Synthesis of cellulose-based carbon dots for bioimaging. *ChemistrySelect* **2016**, *1*, 1314–1317. [CrossRef]

43. Liu, H.; Li, R.S.; Zhou, J.; Huang, C.Z. Branched polyethylenimine-functionalized carbon dots as sensitive and selective fluorescent probes for N-acetylcysteine via an off–on mechanism. *Analyst* **2017**, *142*, 4221–4227. [CrossRef]

44. Behnam, B.; Shier, W.T.; Nia, A.H.; Abnous, K.; Ramezani, M. Non-covalent functionalization of single-walled carbon nanotubes with modified polyethyleneimines for efficient gene delivery. *Int. J. Pharm.* **2013**, *454*, 204–215. [CrossRef]

45. Chen, Y.; Yang, Q.; Xu, P.; Sun, L.; Sun, D.; Zhuo, K. One-step synthesis of acidophilic highly-photoluminescent carbon dots modified by ionic liquid from polyethylene glycol. *ACS Omega* **2017**, *2*, 5251–5259. [CrossRef]

46. Wang, C.; Xu, Z.; Zhang, C. Polyethyleneimine-functionalized fluorescent carbon dots: Water stability, pH sensing, and cellular imaging. *ChemNanoMat* **2015**, *1*, 122–127. [CrossRef]

47. Sonthanasamy, R.S.A.; Fazry, S.; Yamin, B.M.; Lazim, A.M. Surface functionalization of highly luminescent carbon nanodots from *Dioscorea hispida* with polyethylene glycol and branched polyethyleneimine and their in vitro study. *J. King Saud Univ. Sci.* **2019**, *31*, 768–779. [CrossRef]

48. Kang, Y.F.; Li, Y.H.; Fang, Y.W.; Xu, Y.; Wei, X.M.; Yin, X.B. Carbon quantum dots for zebrafish fluorescence imaging. *Sci. Rep.* **2015**, *5*, 11835. [CrossRef] [PubMed]

49. Hutton, G.A.M.; Martindale, B.C.M.; Reisner, E. Carbon dots as photosensitisers for solar-driven catalysis. *Chem. Soc. Rev.* **2017**, *46*, 6111–6123. [CrossRef]

50. Liu, Y.; Wang, P.; Fernando, K.A.S.; LeCroy, G.E.; Maimaiti, H.; Harruff-Miller, B.A.; Lewis, W.K.; Bunker, C.E.; Hou, Z.L.; Sun, Y.P. Enhanced fluorescence properties of carbon dots in polymer films. *J. Mater. Chem. C* **2016**, *4*, 6967–6974. [CrossRef]

51. Liu, J.H.; Cao, L.; LeCroy, G.E.; Wang, P.; Meziani, M.J.; Dong, Y.; Liu, Y.; Luo, P.G.; Sun, Y.P. Carbon "quantum" dots for fluorescence labeling of cells. *ACS Appl. Mater. Interfaces* **2015**, *7*, 19439–19445. [CrossRef]

52. Liu, Y.; Jiang, L.; Li, B.; Fan, X.; Wang, W.; Liu, P.; Xu, S.; Luo, X. Nitrogen doped carbon dots: Mechanism investigation and their application for label free CA125 analysis. *J. Mater. Chem. B* **2019**, *7*, 3053–3058. [CrossRef]

53. Liu, X.; Liu, J.; Zheng, B.; Yan, L.; Dai, J.; Zhuang, Z.; Du, J.; Guo, Y.; Xiao, D. N-doped carbon dots: Green and efficient synthesis on a large-scale and their application in fluorescent pH sensing. *New J. Chem.* **2017**, *41*, 10607–10612. [CrossRef]

54. Qu, D.; Zheng, M.; Du, P.; Zhou, Y.; Zhang, L.; Li, D.; Tan, H.; Zhao, Z.; Xie, Z.; Sun, Z. Highly luminescent S, N co-doped graphene quantum dots with broad visible absorption bands for visible light photocatalysts. *Nanoscale* **2013**, *5*, 12272–12277. [CrossRef]

55. RanguMagar, A.B.; Chhetri, B.P.; Parameswaran-Thankam, A.; Watanabe, F.; Sinha, A.; Kim, J.-W.; Saini, V.; Biris, A.S.; Ghosh, A. Nanocrystalline cellulose-derived doped carbonaceous material for rapid mineralization of nitrophenols under visible light. *ACS Omega* **2018**, *3*, 8111–8121. [CrossRef]

56. Wang, H.X.; Xiao, J.; Yang, Z.; Tang, H.; Zhu, Z.T.; Zhao, M.; Liu, Y.; Zhang, C.; Zhang, H.L. Rational design of nitrogen and sulfur co-doped carbon dots for efficient photoelectrical conversion applications. *J. Mater. Chem. A* **2015**, *3*, 11287–11293. [CrossRef]

57. Diaz-Uribe, C.; Vallejo, W.; Ramos, W. Methylene blue photocatalytic mineralization under visible irradiation on TiO$_2$ thin films doped with chromium. *Appl. Surf. Sci.* **2014**, *319*, 121–127. [CrossRef]

58. Li, S.H.; Wang, R.; Tang, Z.R.; Xu, Y.J. Efficient visible-light-driven water remediation by 3D graphene aerogel-supported nitrogen-doped carbon quantum dots. *Catal. Today* **2019**, *335*, 160–165. [CrossRef]

59. Di, G.; Zhu, Z.; Dai, Q.; Zhang, H.; Shen, X.; Qiu, Y.; Huang, Y.; Yu, J.; Yin, D.; Küppers, S. Wavelength-dependent effects of carbon quantum dots on the photocatalytic activity of g-C$_3$N$_4$ enabled by LEDs. *Chem. Eng. J.* **2020**, *379*, 122296. [CrossRef]

60. Qu, D.; Liu, J.; Miao, X.; Han, M.; Zhang, H.; Cui, Z.; Sun, S.; Kang, Z.; Fan, H.; Sun, Z. Peering into water splitting mechanism of g-C$_3$N$_4$-carbon dots metal-free photocatalyst. *Appl. Catal. B* **2018**, *227*, 418–424. [CrossRef]

61. Kasprzyk, W.; Świergosz, T.; Bednarz, S.; Walas, K.; Bashmakova, N.V.; Bogdał, D. Luminescence phenomena of carbon dots derived from citric acid and urea–a molecular insight. *Nanoscale* **2018**, *10*, 13889–13894. [CrossRef]

62. Ong, W.J.; Tan, L.L.; Ng, Y.H.; Yong, S.T.; Chai, S.P. Graphitic carbon nitride (g-C$_3$N$_4$)-based photocatalysts for artificial photosynthesis and environmental remediation: Are we a step closer to achieving sustainability? *Chem. Rev.* **2016**, *116*, 7159–7329. [CrossRef]

63. Chidhambaram, N.; Ravichandran, K. Single step transformation of urea into metal-free g-C$_3$N$_4$ nanoflakes for visible light photocatalytic applications. *Mater. Lett.* **2017**, *207*, 44–48. [CrossRef]

64. Qu, D.; Zheng, M.; Zhang, L.; Zhao, H.; Xie, Z.; Jing, X.; Haddad, R.E.; Fan, H.; Sun, Z. Formation mechanism and optimization of highly luminescent N-doped graphene quantum dots. *Sci. Rep.* **2014**, *4*, 5294. [CrossRef]

65. Martin, D.J.; Qiu, K.; Shevlin, S.A.; Handoko, A.D.; Chen, X.; Guo, Z.; Tang, J. Highly efficient photocatalytic H$_2$ evolution from water using visible light and structure-controlled graphitic carbon nitride. *Angew. Chem. Int. Ed.* **2014**, *53*, 9240–9245. [CrossRef]

66. Wang, Q.; Huang, J.; Sun, H.; Zhang, K.-Q.; Lai, Y. Uniform carbon dots@TiO$_2$ nanotube arrays with full spectrum wavelength light activation for efficient dye degradation and overall water splitting. *Nanoscale* **2017**, *9*, 16046–16058. [CrossRef]

67. Shi, W.; Guo, F.; Zhu, C.; Wang, H.; Li, H.; Huang, H.; Liu, Y.; Kang, Z. Carbon dots anchored on octahedral CoO as a stable visible-light-responsive composite photocatalyst for overall water splitting. *J. Mater. Chem. A* **2017**, *5*, 19800–19807. [CrossRef]

68. Liu, C.; Fu, Y.; Xia, Y.; Zhu, C.; Hu, L.; Zhang, K.; Wu, H.; Huang, H.; Liu, Y.; Xie, T.; et al. Cascaded photo-potential in a carbon dot-hematite system driving overall water splitting under visible light. *Nanoscale* **2018**, *10*, 2454–2460. [CrossRef]

69. Zhao, S.; Li, C.; Wang, L.; Liu, N.; Qiao, S.; Liu, B.; Huang, H.; Liu, Y.; Kang, Z. Carbon quantum dots modified MoS$_2$ with visible-light-induced high hydrogen evolution catalytic ability. *Carbon* **2016**, *99*, 599–606. [CrossRef]

70. Hang, D.R.; Sun, D.-Y.; Chen, C.H.; Wu, H.F.; Chou, M.M.C.; Islam, S.E.; Sharma, K.H. Facile bottom-up preparation of WS$_2$-based water-soluble quantum dots as luminescent probes for hydrogen peroxide and glucose. *Nanoscale Res. Lett.* **2019**, *14*, 271. [CrossRef] [PubMed]

71. Nandi, S.; Bhunia, S.K.; Zeiri, L.; Pour, M.; Nachman, I.; Raichman, D.; Lellouche, J.P.M.; Jelinek, R. Bifunctional carbon-dot-WS$_2$ nanorods for photothermal therapy and cell imaging. *Chem. Eur. J.* **2017**, *23*, 963–969. [CrossRef] [PubMed]

72. Pan, D.; Zhang, J.; Li, Z.; Wu, C.; Yan, X.; Wu, M. Observation of pH-, solvent-, spin-, and excitation-dependent blue photoluminescence from carbon nanoparticles. *Chem. Commun.* **2010**, *46*, 3681–3683. [CrossRef]

73. Jin, S.H.; Kim, D.H.; Jun, G.H.; Hong, S.H.; Jeon, S. Tuning the photoluminescence of graphene quantum dots through the charge transfer effect of functional groups. *ACS Nano* **2013**, *7*, 1239–1245. [CrossRef]

74. Fu, J.; Yu, J.; Jiang, C.; Cheng, B. g-C$_3$N$_4$-based heterostructured photocatalysts. *Adv. Energy Mater.* **2018**, *8*, 1701503. [CrossRef]

75. Ran, J.; Ma, T.Y.; Gao, G.; Du, X.W.; Qiao, S.Z. Porous P-doped graphitic carbon nitride nanosheets for synergistically enhanced visible-light photocatalytic H$_2$ production. *Energy Environ. Sci.* **2015**, *8*, 3708–3717. [CrossRef]

76. Mosconi, D.; Mazzier, D.; Silvestrini, S.; Privitera, A.; Marega, C.; Franco, L.; Moretto, A. Synthesis and photochemical applications of processable polymers enclosing photoluminescent carbon quantum dots. *ACS Nano* **2015**, *9*, 4156–4164. [CrossRef] [PubMed]

77. Emanuele, A.; Cailotto, S.; Campalani, C.; Branzi, L.; Raviola, C.; Ravelli, D.; Cattaruzza, E.; Trave, E.; Benedetti, A.; Selva, M.; et al. Precursor-dependent photocatalytic activity of carbon dots. *Molecules* **2019**, *25*, 101. [CrossRef] [PubMed]

78. Cailotto, S.; Mazzaro, R.; Enrichi, F.; Vomiero, A.; Selva, M.; Cattaruzza, E.; Cristofori, D.; Amadio, E.; Perosa, A. Design of carbon dots for metal-free photoredox catalysis. *ACS Appl. Mater. Interfaces* **2018**, *10*, 40560–40567. [CrossRef] [PubMed]

79. Su, T.; Shao, Q.; Qin, Z.; Guo, Z.; Wu, Z. Role of interfaces in two-dimensional photocatalyst for water splitting. *ACS Catal.* **2018**, *8*, 2253–2276. [CrossRef]

80. Mehta, A.; Mishra, A.; Basu, S.; Shetti, N.P.; Reddy, K.R.; Saleh, T.A.; Aminabhavi, T.M. Band gap tuning and surface modification of carbon dots for sustainable environmental remediation and photocatalytic hydrogen production—A review. *J. Environ. Manag.* **2019**, *250*, 109486. [CrossRef]

81. Wang, X.; Jiang, X.; Sharman, E.; Yang, L.; Li, X.; Zhang, G.; Zhao, J.; Luo, Y.; Jiang, J. Isolating hydrogen from oxygen in photocatalytic water splitting with a carbon-quantum-dot/carbon-nitride hybrid. *J. Mater. Chem. A* **2019**, *7*, 6143–6148. [CrossRef]

82. Panagopoulos, V.; Zinonos, I.; Leach, D.A.; Hay, S.J.; Liapis, V.; Zysk, A.; Ingman, W.V.; DeNichilo, M.O.; Evdokiou, A. Uncovering a new role for peroxidase enzymes as drivers of angiogenesis. *Int. J. Biochem. Cell. B* **2015**, *68*, 128–138. [CrossRef]

83. Wei, S.-C.; Lin, Y.W.; Chang, H.-T. Carbon dots as artificial peroxidases for analytical applications. *J. Anal. Test.* **2019**, *3*, 191–205. [CrossRef]

84. Nirala, N.R.; Khandelwal, G.; Kumar, B.; Prakash, R.; Kumar, V. One step electro-oxidative preparation of graphene quantum dots from wood charcoal as a peroxidase mimetic. *Talanta* **2017**, *173*, 36–43. [CrossRef]

85. Yang, W.; Huang, T.; Zhao, M.; Luo, F.; Weng, W.; Wei, Q.; Lin, Z.; Chen, G. High peroxidase-like activity of iron and nitrogen co-doped carbon dots and its application in immunosorbent assay. *Talanta* **2017**, *164*. [CrossRef]

86. Wang, B.; Chen, Y.; Wu, Y.; Weng, B.; Liu, Y.; Li, C.M. Synthesis of nitrogen- and iron-containing carbon dots, and their application to colorimetric and fluorometric determination of dopamine. *Microchim. Acta* **2016**, *183*, 2491–2500. [CrossRef]

87. Shi, W.; Wang, Q.; Long, Y.; Cheng, Z.; Chen, S.; Zheng, H.; Huang, Y. Carbon nanodots as peroxidase mimetics and their applications to glucose detection. *Chem. Commun.* **2011**, *47*, 6695–6697. [CrossRef] [PubMed]

88. Lin, Y.; Zhou, Q.; Tang, D.; Niessner, R.; Knopp, D. Signal-on photoelectrochemical immunoassay for aflatoxin B1 based on enzymatic product-etching MnO_2 nanosheets for dissociation of carbon dots. *Anal. Chem.* **2017**, *89*, 5637–5645. [CrossRef] [PubMed]

89. Zhang, J.; Lu, X.; Tang, D.; Wu, S.; Hou, X.; Liu, J.; Wu, P. Phosphorescent carbon dots for highly efficient oxygen photosensitization and as photo-oxidative nanozymes. *ACS Appl. Mater. Interfaces* **2018**, *10*, 40808–40814. [CrossRef] [PubMed]

90. Marković, Z.M.; Kováčová, M.; Humpolíček, P.; Budimir, M.D.; Vajďák, J.; Kubát, P.; Mičušík, M.; Švajdlenková, H.; Danko, M.; Capáková, Z.; et al. Antibacterial photodynamic activity of carbon quantum dots/polydimethylsiloxane nanocomposites against *Staphylococcus aureus*, *Escherichia coli* and *Klebsiella pneumoniae*. *Photodiagnosis Photodyn. Ther.* **2019**, *26*, 342–349. [CrossRef] [PubMed]